Ionic States of Substrates and Transition State Analogues at the Catalytic Sites of *N*-Ribosyltransferases†

Anthony A. Sauve,‡,§ Sean M. Cahill,‡,§ Stephan G. Zech,|| Luiz A. Basso,⊥ Andrzej Lewandowicz,‡ Diogenes S. Santos,⊥ Charles Grubmeyer,# Gary B. Evans,▽ Richard H. Furneaux,▽ Peter C. Tyler,▽ Ann McDermott,|| Mark E. Girvin,‡ and Vern L. Schramm*,‡

Department of Biochemistry, Albert Einstein College of Medicine, 1300 Morris Park Avenue, Bronx, New York 10461, Department of Chemistry, Columbia University, New York, 10027, Departmento de Biologia Molecular e Biotecnologia, Universidade Federal do Rio Grande do Sul, Porto Alegre-RS 91501-970 Brazil, Department of Biochemistry and Fels Research Institute, Temple University School of Medicine, Philadelphia Pa 19140, and Carbohydrate Chemistry Team, Industrial Research Limited, Lower Hutt, New Zealand

Received January 2, 2003; Revised Manuscript Received February 14, 2003

ABSTRACT: Purine nucleoside phosphorylase (PNP) and hypoxanthine-guanine phosphoribosyltransferase (HGPRTase) catalyze N-ribosidic bond cleavage in purine nucleosides and nucleotides, with addition of phosphate or pyrophosphate to form phosphorylated α-D-ribose products. The transition states have oxacarbenium ion character with a positive charge near 1′-C and ionic stabilization from nearby phosphoryl anions. Immucillin-H (ImmH) and Immucillin-H 5′-PO_4 (ImmHP) resemble the transition state charge when protonated at 4′-N and bind tightly to these enzymes with K_d values of 20 pM to 1 nM. It has been proposed that Immucillins bind as the 4′-N neutral form and are protonated in the slow-onset step. Solution and solid-state NMR spectra of ImmH, ImmHP, guanosine, and GMP in complexes with two PNPs and a HGPRTase have been used to characterize their ionization states. Results with PNP•ImmH•PO_4 and HGPRTase•ImmHP•$MgPP_i$ indicate protonation at N-4′ for the tightly bound inhibitors. The 1′-^{13}C and 1′-^{1}H resonances of bound Immucillins showed large downfield shifts as compared to Michaelis complexes, suggesting distortion of 1′-C toward sp^2 geometry. The Immucillins act as transition state mimics by binding with neutral iminoribitol groups followed by 4′-N protonation during slow-onset inhibition to form carbocationic mimics of the transition states. The ability of the Immucillins to mimic both substrate and transition state features contributes to their capture of transition state binding energy. Enzyme-activated phosphoryl nucleophiles bound to PNP and HGPRTase suggest enhanced electrostatic stabilization of the cationic transition states. Distortion of the oxacarbenium ion mimic toward transition state geometry is a common feature of the three distinct enzymatic complexes analyzed here. Substrate complexes, even in catalytically cycling equilibrium mixtures, do not reveal similar distortions.

Purine nucleoside phosphorylase (PNP)[1] and hypoxanthine-guanine-phosphoribosyl transferase (HGPRTase) are purine salvage enzymes that specifically catalyze reversible C-1′ to N-9 bond cleavage between ribose sugars and purine bases (Scheme 1). The enzymes are targets for anti-protozoan therapy because the parasites—including those causing malaria—are purine auxotrophs (*1*−*5*). In humans, PNP inhibition induces apoptosis in activated T-cells, suggesting a clinical means to ameliorate disorders linked to T-cell proliferation (*6*−*8*). Studies on PNP and related phosphoribosyltransferases indicate that catalytic acceleration is achieved through formation of a transition state with oxac-

Scheme 1: Reactions Catalyzed by PNP (A) and HGPRTase (B)[a]

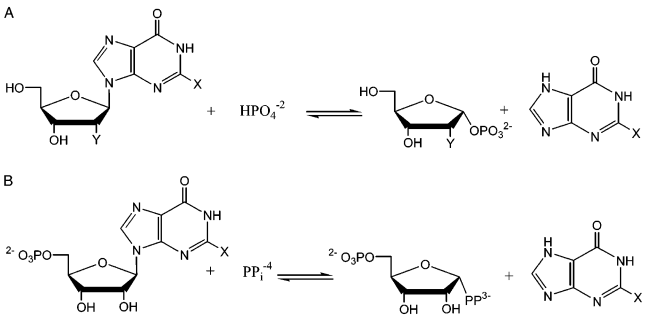

[a] X = H or NH_2, Y = H or OH.

† Supported by research awards from the NIH, the New Zealand Foundation for Research, Science & Technology, the Millenium/CNPq/MCT of Brazil, and the Alexander-von-Humboldt Foundation.

* Address correspondence to the following author. E-mail: vern@aecom.yu.edu. Phone: (718) 430-2813. Fax: (718) 430-8565.

‡ Albert Einstein College of Medicine.

§ Equal contributors to this work.

|| Columbia University.

⊥ Universidade Federal do Rio Grande do Sul.

Temple University School of Medicine.

▽ Industrial Research Limited.

[1] Abbreviations: PNP, purine nucleoside phosphorylase; HGPRTase, hypoxanthine-guanine phosphoribosyltransferase; ImmH, Immucillin-H; ImmHP, Immucillin-H 5′-phosphate; GMP, guanosine 5′-phosphate; IMP, inosine 5′-phosphate; PRPP, 5-phosphoribosyl 1-pyrophosphate; R-1-P, α-D-ribose 1-phosphate; HMQC, heteronuclear multiple quantum correlation; HMBC, heteronuclear multiple bond correlation; HSQC, heteronuclear single-quantum coherence; CP, cross-polarization; MAS, magic-angle spinning; DCP, double cross-polarization.

10.1021/bi034003a CCC: $25.00
Published on Web 04/23/2003

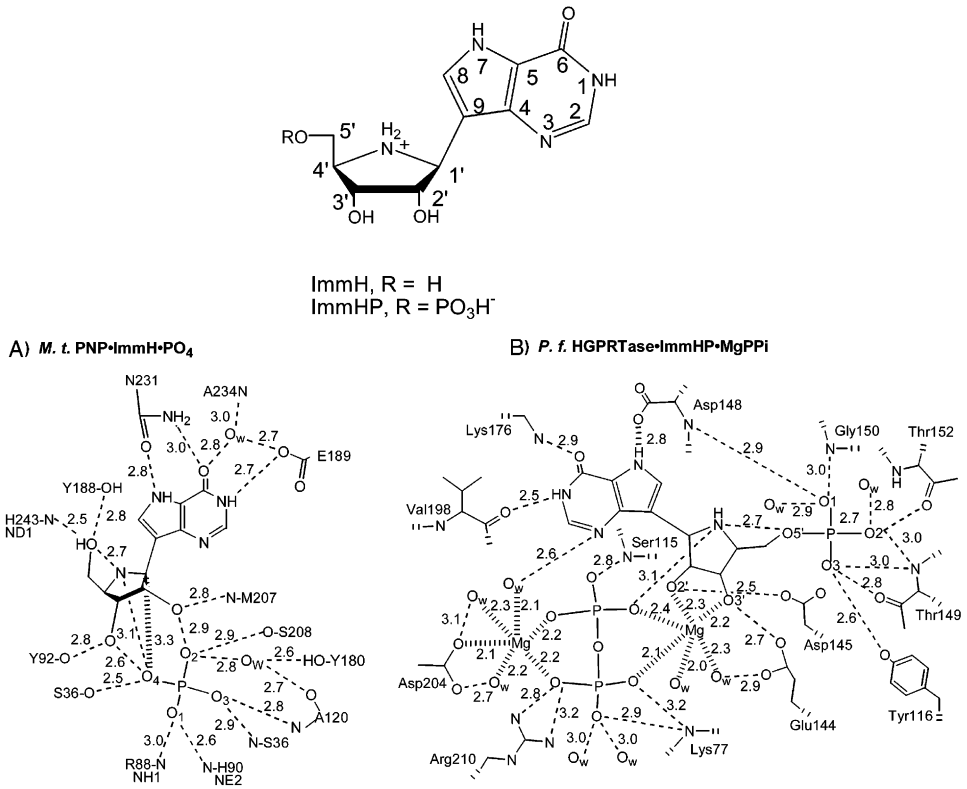

FIGURE 1: Chemical structures of ImmH and ImmH 5′-phosphate (upper panel). The lower panel indicates the catalytic site contacts for ImmH and phosphate at the catalytic site of *M. tuberculosis* PNP (A) and for ImmHP and MgPPi at the catalytic sites of *P. falciparum* HGPRTase (B) (*15*, *18*).

arbenium ion character (*9*−*12*). After the transition state is achieved, the ribosyl electrophile migrates from the purine leaving group to a phosphoryl nucleophile at the catalytic site (*12*). Immucillins incorporate features of the proposed transition states and are potent inhibitors of purine nucleoside phosphorylase (*4*, *6*, *13*−*15*), purine nucleoside hydrolase (*16*), and HGPRTase (*17*−*19*). ImmH (Figure 1, refs *20*−*22*) binds with pM affinity to the PNPs from bovine, human, *Plasmodium falciparum*, and *Mycobacterium tuberculosis* (refs *4*, *6*, *13*, *14*; Figure 1), and ImmHP binds to *P. falciparum* and other protozoan HGPRTases with K_i values near 1 nM, about 10^4 times more tightly than their nucleotide substrates (*18*, *19*).

The 9-deaza feature of the Immucillins elevates the pK_a at 7-N, and 4′-N has a pK_a that permits formation of the cation at neutral pH. Protonation at 7-N captures a hydrogen bond to the enzyme that is a feature of the transition states but not the Michaelis complexes. This interaction has been identified by X-ray crystallography and NMR spectroscopy in complexes of PNP•ImmH•PO_4 and HGPRTase•ImmHP•$MgPP_i$ (refs *12*, *15*, *17*−*19*; Figure 1). In principle, the Immucillins can bind as the 4′-N neutral form like the substrate or as the 4′-N cationic form resembling the oxacarbenium ion of the transition state. Iminoribitol transition state analogues bind to PNP and to nucleoside *N*-ribosyl hydrolases as the neutral species, and it has been postulated that a subsequent step forms the cation (*14*, *23*). The ionization state of Immucillins following slow-onset inhibition has not been established but is critical to an understanding of the tight binding of these inhibitors (*12*, *15*, *17*, *18*). Here, we provide solution and solid-state NMR evidence that [1′-^{13}C, 4′-^{15}N]ImmH bound to PNPs (of both *M. tuberculosis* and human origin) and [1′-^{13}C, 4′-^{15}N]ImmHP bound to *Tritrichomonas foetus* HGPRTase are N-4′ protonated to behave as mimics of the oxacarbenium ion transition states. The phosphoryl groups found in these complexes appear to be highly nucleophilic from their ^{31}P chemical shifts. NMR analysis of free and bound Immucillins indicates that in these complexes, mimicry of transition state features is a dominant force for tight binding. In contrast, Michaelis complexes show relatively little reactant state destabilization.

MATERIALS AND METHODS

Materials. ImmH and ImmHP were synthesized as reported (*21*). [1′-^{13}C, 4-^{15}N]ImmH was synthesized from [1-^{13}C]-D-gulonolactone utilizing the method of Fleet and Son (*37*) except that [^{15}N]-benzylamine was used. [1-^{13}C]-D-Gulonolactone was prepared via a known procedure using [^{13}C]NaCN (*38*). Phosphorylation of these compounds using $POCl_3$ and trimethyl phosphate was performed as reported previously (*17*). Recombinant *M. tuberculosis* purine nucleoside phosphorylase was produced in recombinant form in a bacterial system as reported (*14*). Similarly, *T. foetus* HGPRTase was produced and purified as reported (*24*). Human PNP was recloned into pCRT7/NT-TOPO with an N-terminal His_6-tag vector for ease of expression in *Escherichia coli* and purification. For solid-state NMR, internal protein label was provided by growth of overexpressing cells on 200 mg/L [2-^{13}C, ^{15}N]glycine and incorporation confirmed by MS and NMR. Full details of cloning, expression, and purification will be presented elsewhere. Solution NMR measurements for proteins, inhibitors and protein−ligand complexes were obtained on either 300 or 600 MHz Bruker instruments. All buffers were obtained in the highest purities available and used as received. Magnesium chloride was 99.9% pure and was obtained from Sigma.

Solution NMR Experiments. 1-D proton spectra were typically collected using WATERGATE water suppression (*39*) on the Bruker 600 MHz instrument using 64 scans, a sweep width of 14 ppm sampled with 1024 complex points, and a recycle delay of 1.3 s. Spectra were processed with a cosine bell window function, were zero filled to 2048 points, and were baseline corrected after Fourier transformation. 2-D ^{1}H ^{13}C gradient selected sensitivity-enhanced HSQC spectra were typically collected with 1024 and 32 complex points in t_2 (^{1}H) and t_1 (^{13}C), respectively, on the Bruker 600 MHz instrument, with 32 scans per t_1 point and a recycle delay of 1.3 s. All experiments used a proton sweep width of 14 ppm and a ^{13}C sweep width of 40 ppm with the ^{1}H and ^{13}C carriers set to 4.7 and 50 ppm, respectively. The proton dimension was zero filled to 2048 points, and the ^{13}C dimension was linear predicted to 128 points before processing with a cosine bell window function in each dimension.

1-D ^{31}P spectra were typically collected using continuous proton-decoupling on the Bruker 300 MHz instrument with 10 000 scans, a 30° pulse, a 50 ppm sweep width centered at 0 ppm and sampled with 4096 complex points, and a recycle delay of 1.5 s. Spectra were processed with a 1 Hz exponential window function, were zero filled to 16 K points, and were baseline corrected after Fourier transformation.

1-D ^{15}N spectra were typically collected using continuous proton-decoupling on the Bruker 300 MHz instrument with 100 000 scans, a 30° pulse, a 105 ppm sweep width centered at 75 ppm and sampled with 2048 complex points, and a recycle delay of 1.5 s. Spectra were processed with a 10 Hz exponential window function, were zero filled to 16 K points, and were baseline corrected after Fourier transformation. Proton chemical shifts were referenced to internal 3-(trimethylsilyl)propionate. ^{15}N and ^{13}C chemical shifts were referenced indirectly from the proton chemical shift reference (*40*).

Chemical Titration of ImmH. A 5 mL solution of ImmH at a concentration of 50 mM was used to obtain the acid−base titration with a 5 M solution of NaOH as a titrant. The pH of the solution was measured after each addition of base. Each base addition was 2 μL. A total of 175 μL was added, and the pH varied from 1 to 11. A plot of base added in equivalents versus pH was constructed from the data, and the plot was used to assign the number of titratable protons and the pH values of the buffer regions. A similar solution containing 10% MeOH was shown to be nearly identical when titrated. Spectra were collected at 300 MHz and at 25 °C.

NMR Studies of ImmH in the Range of pH 1−10. Measurement of ^{1}H, ^{13}C and ^{15}N chemical shifts as a function of pH were made using 2-D ^{1}H, ^{13}C-HMQC, 2-D ^{1}H, ^{13}C-HMBC, and 2-D ^{1}H, ^{15}N-HMBC experiments on the Bruker 300 MHz instrument. 2-D ^{1}H, ^{15}N gradient-selected HMBC experiments were collected with 1024 and 64 complex points in t_2 (^{1}H) and t_1 (^{15}N), respectively, with 8 scans per t_1 point and a recycle delay of 1.5 s. The experiments used a proton sweep width of 14 ppm and a ^{15}N sweep width of 120 ppm with the ^{1}H and ^{15}N carriers set to 4.7 and 60 ppm, respectively. The proton dimension was zero filled to 2048 points, and the ^{15}N dimension was linear-predicted to 256 points before processing with a sine bell window function in each dimension. 2-D ^{1}H ^{13}C gradient-selected HMBC experiments were collected with 1024 and 64 complex points in t_2 (^{1}H) and t_1 (^{13}C), respectively, with 128 scans per t_1 point and a recycle delay of 1.5 s. The experiments used a proton sweep width of 14 ppm and a ^{13}C sweep width of 220 ppm with the ^{1}H and ^{13}C carriers set to 4.7 and 100 ppm, respectively. The proton dimension was zero filled to 2048 points, and the ^{13}C dimension was linear-predicted to 256 points before processing with a cosine bell window function in each dimension. 2-D ^{1}H ^{13}C gradient-selected HMQC experiments were collected with 1024 and 64 complex points in t_2 (^{1}H) and t_1 (^{13}C), respectively, with 32 scans per t_1 point and a recycle delay of 1.5 s. The experiments used a proton sweep width of 14 ppm and a ^{13}C sweep width of 170 ppm with the ^{1}H and ^{13}C carriers set to 4.7 and 75 ppm, respectively. The proton dimension was zero filled to 2048 points, and the ^{13}C dimension was linear-predicted to 256 points before processing with a cosine bell window function in each dimension.

A 5 mM sample of [1′-^{13}C, 4′-^{15}N]ImmH was dissolved in 10% MeOD-d_4/90% D_2O. The methanol was added to reduce precipitation of ImmH in the pH range of 6−9. Increments of 2 M NaOD were added, and the pH was measured by a micro pH-electrode that was inserted into the NMR tube. A set of spectra including a 1-D ^{1}H; ^{1}H, ^{13}C-HMQC; ^{1}H, ^{15}N-HMBC; and ^{1}H, ^{13}C-HMBC were obtained for each addition of base. For the pH range from 4 to 8.8, all nuclear spins of the ImmH molecule were assigned at base increments of 0.15 equiv to fully map the chemical shift change as the acidic protons were titrated. Chemical shift changes were also determined at the extremes of pH that overlap for removal or addition of protons to the purine ring. The pH values were achieved by DCl addition or excess addition of NaOH. Similar titrations of ImmH were performed in DMSO-d_6. Chemical shift changes for ImmHP and ImmH were also measured in solutions containing 30% DMSO-d_6/70% D_2O. In the single equivalent base titration shown in Figure 4, 10 μmol of [1′-^{13}C, 4′-^{15}N]ImmH•HCl was added to 1 mL of DMSO-d_6, and an NMR spectrum was obtained. After this, 10 μmol of sodium ethoxide was added dissolved in 25 μL of DMSO-d_6, and a second NMR spectrum was obtained. Spectra were collected at 25 °C at 300 MHz. Addition of methanol and DMSO up to 20% caused only slight changes (<1 ppm) from the original assignments.

NMR Investigation of PNPase, [1′-^{13}C, 4′-^{15}N]ImmH, and Phosphate. A 1 mM (monomer) solution of *M. tuberculosis* PNP was prepared buffered with 25 mM potassium phosphate in 90% D_2O, and the pH was adjusted to 7.5 by addition of NaOD. A 1-D ^{1}H NMR spectrum of this sample was obtained prior to the addition of 1 mol equiv of [1′-^{13}C, 4′-^{15}N]ImmH (vs monomer) in a 50 μL volume of D_2O. A subsequent 1-D spectrum was then obtained as before. ^{1}H, ^{13}C-HSQC spectra were obtained at 20, 30, 45, and 60 °C. To identify bound inhibitor signals in the HSQC spectrum, a washout protocol was employed. The sample of PNP•[1′-^{13}C, 4′-^{15}N]ImmH•PO_4 was incubated with a 10-fold excess of unlabeled ImmH in a volume increased 10-fold. After incubation overnight at 37 °C and concentration through a semipermeable membrane, the HSQC spectrum was obtained. The signal located at 6.3 and 67 ppm decreased. New signals from free [1′-^{13}C, 4′-^{15}N]ImmH were attributed to free exchanged ImmH in the sample.

NMR Investigation of HGPRTase, [1′-^{13}C, 4′-^{15}N]ImmHP, and Pyrophosphate. A 1 mM (monomer) solution of HGPRTase was prepared buffered with 25 mM potassium phosphate, 3 mM sodium pyrophosphate, 3 mM $MgCl_2$, and 90% D_2O, and the pH was adjusted to 7.5 by addition of NaOD. A 1-D ^{1}H NMR spectrum of this sample was obtained prior to addition of 1 mol equiv of [1′-^{13}C, 4′-^{15}N]ImmHP (vs monomer) in a 50 μL volume of D_2O. A subsequent 1-D spectrum was then obtained as before. ^{1}H-^{13}C HSQC spectra were obtained at 25 and 30 °C. To establish the identity of inhibitor-specific resonances in the HSQC spectrum, a washout protocol was employed. The labeled ImmHP sample was incubated with a 10-fold excess of unlabeled ImmHP in a volume increased in buffer by 10-fold. After incubation overnight at 37 °C and concentration to original volume, the HSQC spectrum was obtained. A cross-peak at (6.2, 64.5) declined in intensity after the washout procedure. New signals appeared that were attributed to free [1′-^{13}C, 4′-^{15}N]-ImmHP in the sample.

Phosphorus and Nitrogen Spectra. ^{31}P (w/^{1}H decoupling) spectra were obtained by incubation of phosphate, PNP, and ImmH at concentrations of 2 mM or greater in 50 mM phosphate buffer at pH 7.5 (24 000 scans). Conditions for the ^{31}P spectrum of HGPRTase with ImmHP were as follows: 50 mM potassium phosphate pH 7.7, 2 mM PP_i, 2 mM $MgCl_2$, 2 mM HGPRTase, and 1.5 equiv of [1′-^{13}C, 4′-^{15}N]ImmHP (8500 scans). The chemical shifts for ^{31}P spectra were referenced to phosphoric acid.

The ^{15}N spectrum of the same HGPRTase same sample was obtained as 105 000 scans. Washout of the label was done as described above. A ^{1}H, ^{13}C HSQC confirmed washout of label and the control ^{15}N spectrum was recorded (105 000 scans).

HSQC Spectra for PNP with Labeled Guanosine. PNP was concentrated to 3 mM in 80% D_2O 50 mM Tris-d_{11}, pH 7.5 containing 75 mM KCl. 1-D and ^{1}H, ^{13}C HSQC spectra of the protein and protein after addition of 3 mM U-[^{13}C, ^{15}N]-guanosine were acquired, using methods similar to the spectral collection for the ImmH complex. A solution of 50 mM phosphate (pH = 7.5 in D_2O) was then added to a final concentration of 2 mM, and another cycle of spectra was acquired. Addition of 100 μL of 50 mM phosphate containing 50 mM unlabeled guanosine was used to exchange the U-[^{13}C, ^{15}N]guanosine and other labeled products from the enzyme. As a control, the corresponding spectra of free U-[^{13}C, ^{15}N]guanosine at 2 mM were also obtained.

HSQC Spectra for HGPRTase with Labeled GMP. HGPRTase was concentrated to 3 mM in 90% D_2O in 50 mM phosphate, pH 7.5 containing 75 mM KCl. 1-D and ^{1}H, ^{13}C-HSQC spectra of the protein and protein after addition of 3 mM U-[^{13}C, ^{15}N]guanosine-5′-monophosphate were acquired, similar to the spectra obtained for the ImmHP complex. A solution of 50 mM pyrophosphate containing 50 mM $MgCl_2$ (pH = 7.5 in D_2O) was added to a final concentration of 5 mM, and another cycle of spectra were acquired. As a control, the corresponding spectra of free U-[^{13}C, ^{15}N]-guanosine-5-phosphate at 3 mM were also obtained.

Solid-State NMR Sample Preparation. Solid human PNP•ImmH•PO_4 was prepared by dialysis of 35 mg of PNP against 50 mM Tris HCl at pH 7.5 followed by addition of 1.2 μmol of [1′-^{13}C, 4′-^{15}N]ImmH and 6 μmol of potassium phosphate, pH 7.5. After 2 h, the sample was concentrated to 1 mL by ultrafiltration. Addition of 100 μL PEG-400 (50%) to achieve a final PEG concentration of 12.5% caused crystallization after 18 h at 4 °C. Crystalline protein was harvested by rapid centrifugation and packed for NMR experiments. Solid labeled ImmH (protonated) was obtained as a lyophilized solid from HCl at pH 3.0. Solid neutral ImmH was prepared by titration of 1 mL of a 75 mM solution of labeled ImmH containing 5 ppm $CuSO_4$ by addition of concd NaOH. Base titration was completed at pH 8.2 as determined by a pH meter. White semicrystalline material formed in the cold and was spun down and dried in a vacuum for use in NMR experiments.

Solid-State NMR Experiments. Spectra were acquired on a Varian/Chemagnetics Infinity Plus 600 spectrometer operating at 599.4 MHz proton frequency, 150.7 MHz ^{13}C, and 60.4 MHz ^{15}N frequencies using a triple resonance T3 MAS probe (Varian Instruments). The spinning frequency of the 3.2 mm (o.d.) rotor has been adjusted to 8.0 kHz (1-D spectra) or 13.5 kHz (2-D spectra). The sample was cooled to a temperature of 5 °C using dry air. Cross polarization experiments were carried out with a linear ramped rf field on the ^{15}N or ^{13}C channel. Heteronuclear decoupling was applied during acquisition using the TPPM sequence (*41*) with a field strength of about 65 kHz. For 1-D experiments, 1024 points were acquired with a spectral width of 66 kHz. A sinebell apodization function has been applied before zero filling to 2048 points and Fourier transformation. ^{13}C spectra were referenced externally to TMS for ^{13}C using the methylene peak of adamantane at 38.6 ppm. The ^{15}N chemical shift was referenced to liquid NH_3 using the peak at 38.5 ppm in solid $^{15}NH_4Cl$. For the two-dimensional correlation experiments, double cross-polarization (*42*) was implemented selectively (*43*) to direct the polarization transfer from nitrogen to carbon (C-α). For the nitrogen−carbon transfer step, rf field strengths were adjusted to 20.25 MHz for ^{15}N and 33.75 MHz for ^{13}C. 1024 complex points (t_2) and 128 real points (t_1) have been acquired with spectral widths of 66 kHz (w_2) and 10 kHz (w_1), respectively. We thank Chad M. Rienstra for implementing the DCP sequence.

RESULTS

NMR Assignments of pK_a Values for ImmH. Titration of ImmH with a strong base established three ionizable protons, their pK_a values, and related NMR chemical shifts. The pK_a values for titratable protons were 1.4, 6.9, and 10.0, respectively (Figure 2). NMR spectra using 1-D ^{1}H, ^{1}H, ^{13}C-HMQC ^{1}H, ^{13}C-HMBC, and ^{1}H, ^{15}N-HMBC methods were used to assign the pK_a at 1.4 to 3-N and the pK_a at 10.0 to 1-N (Tables 1 and 2). Assignment of the protonation state of the 4′-imino nitrogen was facilitated by analysis of [1′-^{13}C, 4′-^{15}N]ImmH (Figure 3 and Table 1). The chemical shift of ^{15}N changed from 56.7 to 51.2 ppm with the midpoint centered at pH 7.4 (measured by pH meter in D_2O) corresponding to the pK_a of 6.9 observed for titration in H_2O. The protons on 4′-N were observed directly by titration of [1′-^{13}C, 4′-^{15}N]ImmH•HCl in DMSO-d_6. Two signals with ^{15}N coupling (76 Hz, two protons) were converted to a broad signal with addition of 1 equiv of base (Figure 4).

The chemical shifts of 1′-H and 4′-H of ImmH were sensitive to its 4′-N protonation state and decreased by 0.65 and 0.61 ppm, respectively, upon deprotonation (Table 1).

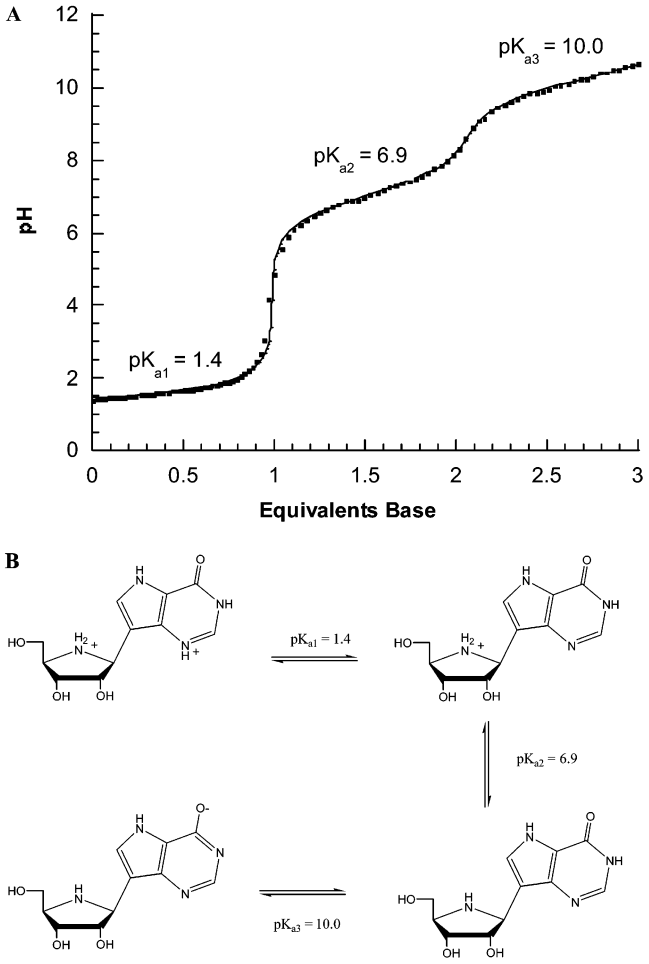

FIGURE 2: Acid salt ImmH•2HCl was titrated by NaOH additions followed by pH measurement. The pK_a assignments are shown in panel B. The pK_a values were determined by use of the half-equivalent pH measurement as determined from the inflection point at full titration of the respective proton.

Table 1: Tabulated Chemical Shifts of ImmH and ImmHP at Different pH Values[a]

	ImmH			ImmHP	
atom	chemical shift (pH 5)	chemical shift (pH 9)	atom	chemical shift (pH 5)	chemical shift (pH 9)
4′-^{15}N	56.7	51.2	4′-^{15}N	57.2	51.5
1′-^{1}H	4.95	4.30	1′-^{1}H	4.93	4.21
4′-^{1}H	3.85	3.24	4′-^{1}H	3.91	3.17
1′-^{13}C	59.6	60.0	1′-^{13}C	57.1	57.7
4′-^{13}C	67.9	67.6	4′-^{13}C	64.5	65.5
9-^{13}C	110.3	117.8	9-^{13}C	106.3	113.5
5′-^{13}C	61.2	64.7	5′-^{13}C	62.7	63.0

[a] Values for the chemical shifts of [4′-^{15}N]ImmH as determined in D_2O (99%). The pH values are pH meter measurements and are not corrected for D_2O content.

In contrast, the 1′-^{13}C and 4′-^{13}C chemical shifts were insensitive to 4′-N deprotonation, but the carbon chemical shifts at the 5′ and 9 positions increased by 3.5 and 7.5 ppm, respectively (Table 1). For ImmHP, the chemical shifts of 4′-^{15}N, 1′-^{13}C, 4′-^{13}C, 5′-^{13}C, 9-^{13}C, 1′-^{1}H, and 4′-^{1}H were similar to those measured for ImmH in the pH range of 5−9 (Table 1). These NMR frequency changes could then be used to assign the 4′-N protonation state of [1′-^{13}C, 4′-^{15}N]-Immucillins at the catalytic sites of PNPs and HGPRTase.

Table 2: Aromatic Chemical Shift Values of ImmH at Different pH Values[a]

atom	ppm (pH 1)	ppm (pH 5)	ppm (pH 9)	ppm (pH 11)
H2	8.9	8.17	8.10	8.02
H8	7.88	7.86	7.68	7.45
C2	145.9	144.5	146.1	153.9
C4	133.8	143.4	145.9	147.0
C5	117.7	117.6	118.8	121.6
C6	152.2	157.3	158.5	163.2
C8	130.8	131.8	130.3	128.8

[a] The experimental conditions for these measurements are similar to those for Table 1 and are fully described in the Materials and Methods.

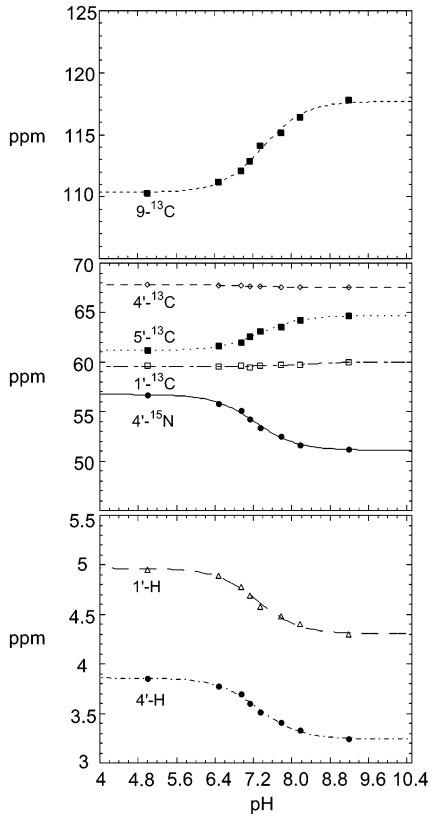

FIGURE 3: pH dependence of ImmH NMR chemical shifts. Spectra were taken in D_2O (95%) at 300 MHz as indicated in Materials and Methods. The solid curves are least-squares fits to the points for titration of a single proton. The pK_a value (in D_2O) determined from all fits is 7.45.

Complexes of ImmH and PO$_4$ with PNP. ImmH is a slow-onset, tight-binding inhibitor for PNP from *M. tuberculosis*. Each monomer of this homotrimer contains a single active site that binds inhibitor independently with a dissociation constant in the pM range (*14*). The 1-D ^{1}H NMR spectra of PNP alone as compared to PNP•[1′-^{13}C, 4′-^{15}N]ImmH•PO$_4$ showed extensive changes, confirming the interaction of inhibitor and protein. Complete inhibition of catalytic activity in the complex also confirmed inhibitor binding.

The signal for bound [1′-^{13}C, 4′-^{15}N]ImmH appeared in the ^{1}H, ^{13}C-HSQC spectra above 30 °C at ^{1}H = 6.3, ^{13}C = 65 ppm (Figure 5). The complex is stable at elevated temperatures, and at 60 °C this signal increased in intensity and shifted to ^{1}H = 6.5, ^{13}C = 66. Addition of a 10-fold excess of unlabeled ImmH diminished the signal from bound [1′-^{13}C, 4′-^{15}N]ImmH, establishing assignment of the cross-

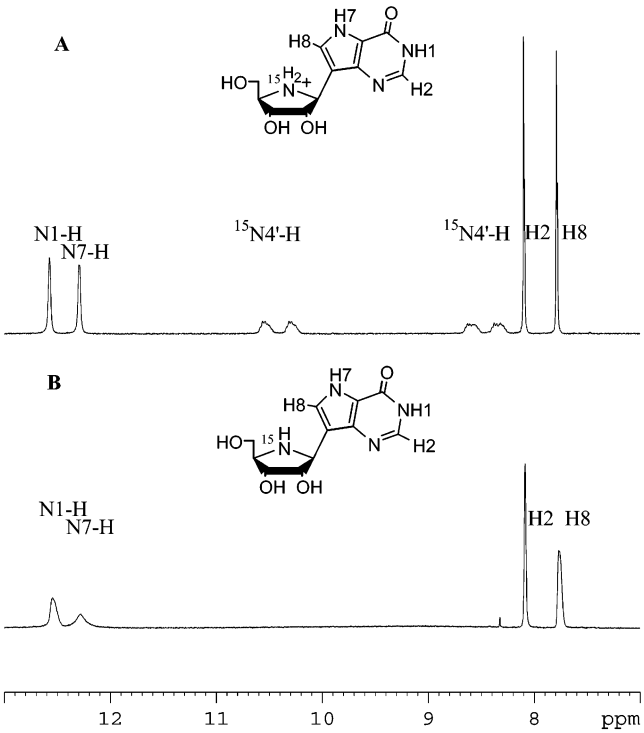

FIGURE 4: NMR of ImmH cation in DMSO-d_6 (A) and ImmH after addition of 1 equiv of sodium ethoxide (B).

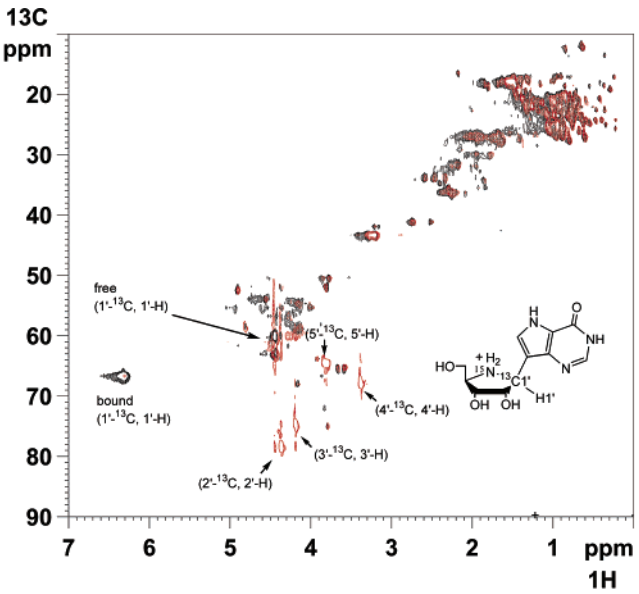

FIGURE 5: ^{1}H, ^{13}C HSQC of PNP•[1′-^{13}C, 4′-^{15}N]ImmH•phosphate (black). HSQC of PNP•[1′-^{13}C, 4′-^{15}N]ImmH•phosphate after addition of excess unlabeled ImmH followed by exchange at 37 °C for 12 h and concentration by ultrafiltration (overlay in red). Spectra were taken at 60 °C.

peak to bound ImmH. The appearance of signals from free [1′-^{13}C, 4′-^{15}N]ImmH at (^{1}H = 4.5, ^{13}C = 59.5) confirmed release from the enzyme (Figure 5). The ^{15}N spectrum of bound ImmH was not resolved in solution NMR.

^{31}P NMR Chemical Shifts of Bound Phosphate. The ^{31}P NMR spectrum from the PNP•ImmH•PO_4 complex gave a large signal at 3.6 ppm assigned to free phosphate and a smaller signal at 4.1 ppm assigned to phosphate anion in the active site (Figure 6B). The chemical shift of 3.6 ppm for free phosphate is anomalously high as compared to free

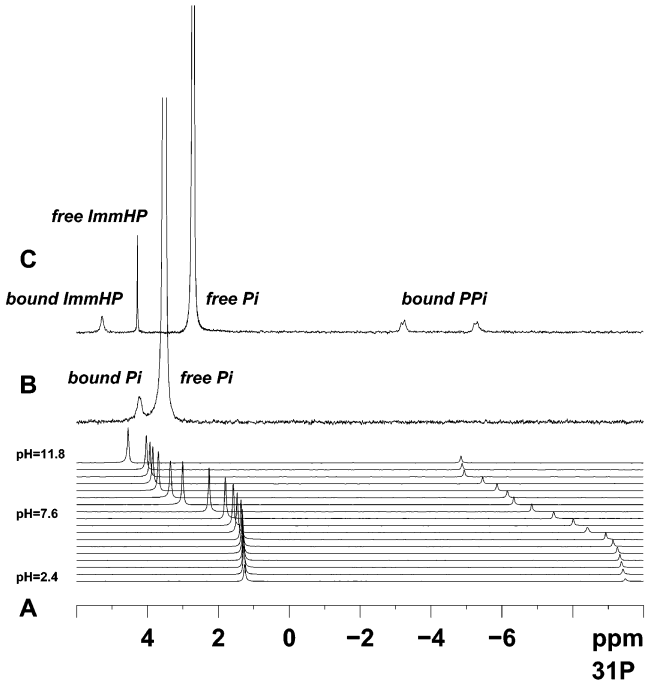

FIGURE 6: ^{31}P NMR spectra. Chemical titration of H_3PO_4 and $H_4P_2O_7$ by base addition monitored by ^{31}P NMR (A). PNP•ImmH• phosphate (same as in Figure 5), with phosphate in excess at 50 mM, pH 7.5 (B). HGPRTase, pyrophosphate, 2.5 mM Mg^{2+}, and 5 mM PP_i and 50 mM P_i buffer (C). Experiments were performed at pH 7.6, 27 °C, and 300 MHz.

phosphate at the same pH and may be due to chemical exchange. The nature of the exchange has not been defined but could arise from the catalytic site or a nonspecific cationic site on the enzyme. The downfield shift of the bound phosphate is consistent with a net charge in excess of −2, equivalent to the chemical shift of free phosphate at a pH of 10.5, or electronic distortion imposed by the catalytic site.

^{1}H, ^{13}C NMR of T. foetus HGPRTase•ImmHP•$MgPP_i$. HGPRTases equilibrate PRPP and hypoxanthine or guanine with inorganic pyrophosphate and IMP or GMP, respectively, in the presence of Mg^{2+} (Scheme 1). HGPRTases from several species have been characterized by crystallography, and here we use NMR to characterize the enzyme from *T. foetus* (*23*−*30*). The *T. foetus* enzyme is a homodimer with subunits of 20 kDa (*27*). The catalytic sites of HGPRTases bind a single ImmHP molecule, pyrophosphate, and two Mg^{2+} ions that sandwich the pyrophosphate (*17*, *18*). Comparison of 1-D NMR spectra of free HGPRTase and HGPRTase•ImmHP•$MgPP_i$ established formation of a stable complex and was verified by enzymatic inhibition (*29*).

The 1′-H and 1′-^{13}C signals of bound [1′-^{13}C, 4′-^{15}N]-ImmHP were shifted downfield (^{1}H = 6.2, ^{13}C = 64.5) from the location of 4′-protonated free ImmHP (^{1}H = 4.9, ^{13}C = 57.5, Figure 7). Assignment of the peak to bound ImmHP was confirmed by addition of excess unlabeled ImmHP to exchange the labeled derivative. Signals for free [1′-^{13}C, 4′-^{15}N]ImmHP appeared in the sample after washout. Binding to HGPRTase causes chemical shift changes of 1.3 ppm for 1′-^{1}H and 7 ppm for 1′-^{13}C. These changes resemble those for [1′-^{13}C, 4′-^{15}N]ImmH bound to PNP (Figure 5).

^{31}P and ^{15}N NMR Spectra of HGPRTase•[1′-^{13}C, 4′-^{15}N]-ImmHP•$MgPP_i$. Signals for ^{31}P were observed for bound

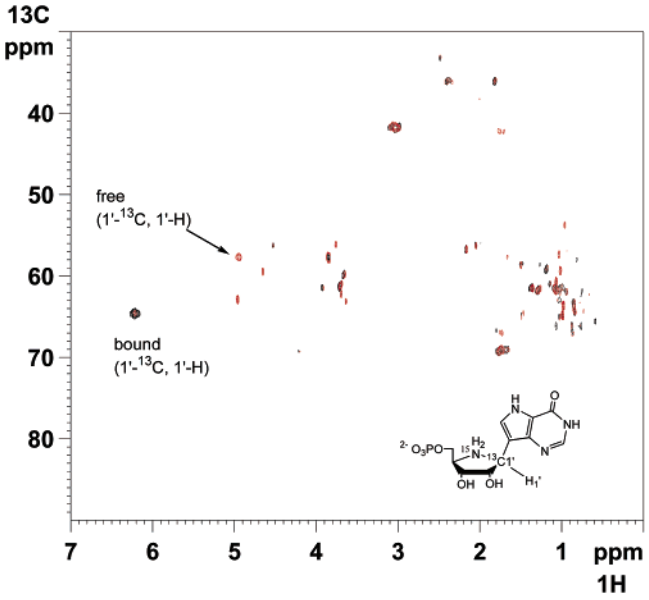

FIGURE 7: ^{1}H, ^{13}C HSQC of HGPRTase and [1′-^{13}C, 4′-^{15}N]ImmHP in the presence of pyrophosphate and Mg^{2+} (black). HSQC of HGPRTase and [1′-^{13}C, 4′-^{15}N]ImmHP in the presence of pyrophosphate after incubation with multiple equivalents of unlabeled buffered ImmHP for 12 h (overlay in red). Experiments were performed at pH 7.6 and 27 °C

pyrophosphate and the 5′-phosphate monoester in the complex HGPRTase•[1′-^{13}C, 4′-^{15}N]ImmHP•$MgPP_i$ (Figure 6A). When compared to the pH titration of free pyrophosphate and phosphate, the ^{31}P NMR spectrum shows the chemical shifts of bound pyrophosphate split into two resonances indicative of different chemical environments equivalent to pH values of >12 and 9.5 for the two phosphate groups. The pyrophosphate phosphoryl at −3 ppm has a chemical shift similar to fully ionized pyrophosphate in solution but will be influenced by chelation with the two Mg^{2+} ions that sandwich PP_i at the catalytic site. Free magnesium-pyrophosphate was not visible in the enzyme experiment because of broadening effects. The chemical shifts of bound pyrophosphate were insensitive to magnesium ion concentration ranging from 1 to 4 equiv. Although direct assignments for proximal and distal groups cannot be made from this experiment, both phosphoryl groups of pyrophosphate exist as Mg^{2+}-chelates at the catalytic site, giving chemical shifts corresponding to highly ionized free PP_i. These interactions are required to generate one nucleophilic oxygen from the asymmetric $(Mg)_2PP_i$ ensemble. The chemical shift of the 5′-phosphate monoester is also downfield in the bound form relative to free solution, reflecting its environment in the complex (Figures 1 and 6A).

The resonance of the 4′-^{15}N of bound [1′-^{13}C, 4′-^{15}N]-ImmHP was visible in the ^{15}N NMR spectrum at 58.9 ppm (Figure 8). The spectra of the HPGPRTase•ImmHP complex before and after exchange with unlabeled ImmHP established that the signal is from bound ImmHP. Comparisons of chemical shifts of bound ImmHP with the corresponding chemical shift of [1′-^{13}C, 4′-^{15}N]ImmHP in cationic (57.2 ppm) and neutral (51.3 ppm) forms indicates that ImmHP is bound to HGPRTase as the cation.

NMR of PNP•U-[^{13}C, ^{15}N]guanosine with M. tuberculosis PNP. Saturation of PNP with guanosine and phosphate forms an equilibrium mixture of guanosine, guanine, PO_4, and

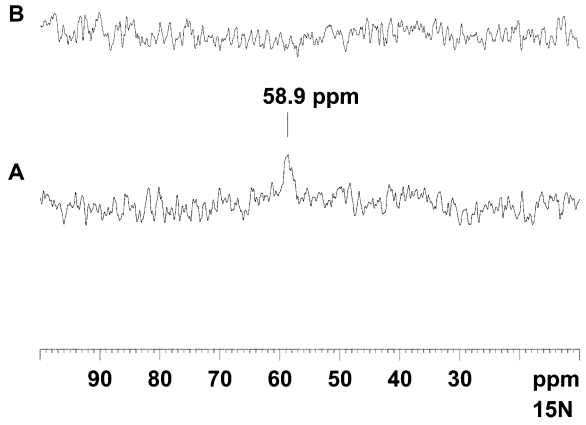

FIGURE 8: ^{15}N 1-D NMR spectra of HGPRTase in complex with [1′-^{13}C, 4′-^{15}N]ImmHP, pyrophosphate, and magnesium chloride before (A) and after (B) washout of labeled ImmHP by incubation with unlabeled ImmHP (see Figure 7). Experiments were performed at pH 7.6 and 27 °C.

Scheme 2: Binding Equilibria of PNP with Guanosine, Phosphate, Ribose-1-Phosphate (R-1-P), and Guanine

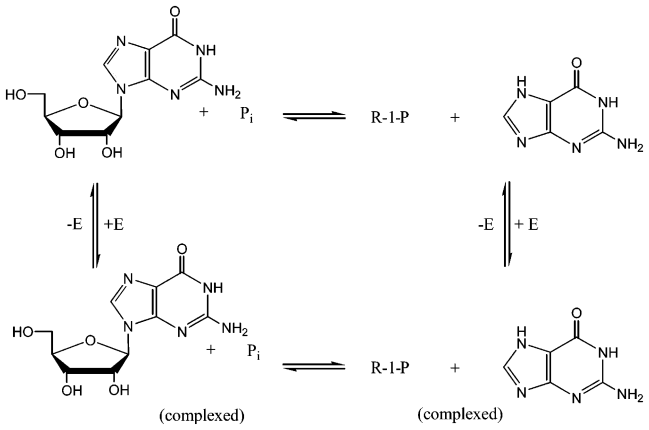

R-1-P on the catalytic sites and in solution (Scheme 2). Chemical shifts can be compared to the complex with bound ImmH and PO_4 to compare interactions with substrates and transition state analogues. HSQC studies of PNP•U-[^{13}C, ^{15}N]-guanosine confirmed that guanosine binds to the enzyme in the absence of phosphate (Figure 9). The chemical shift of the cross-peak for [1′-^{1}H, 1′-^{13}C]guanosine at (^{1}H = 6.2, ^{13}C = 91 ppm) is perturbed only slightly relative to guanosine in solution (^{1}H = 6.05, ^{13}C = 90 ppm). Phosphate addition did not significantly alter the bound guanosine signal but resulted in formation of R-1-P (^{1}H = 5.7, ^{13}C = 101 ppm). Addition of excess unlabeled guanosine and phosphate confirmed the assignments of the free and bound guanosine and R-1-P chemical shifts in that the intensities of unbound U-[^{13}C, ^{15}N]guanosine were enhanced.

NMR Spectra of T. foetus HGPRTase•U-[^{13}C, ^{15}N]GMP. The complex of HGPRTase•U-[^{13}C, ^{15}N]GMP forms in the absence of pyrophosphate, a result previously demonstrated by X-ray crystallography (27). The cross-peak for bound [1′-^{1}H, 1′-^{13}C]GMP was found at (^{1}H = 6.2, ^{13}C = 92 ppm) as compared to the location of the cross-peak for the free nucleotide at (^{1}H = 5.95, ^{13}C = 89 ppm).

Addition of Mg^{2+}-pyrophosphate caused the enzyme to reach a rapid equilibrium involving free and bound GMP and pyrophosphate as well as free and bound guanine and PRPP (Scheme 3). No chemical shift changes were apparent

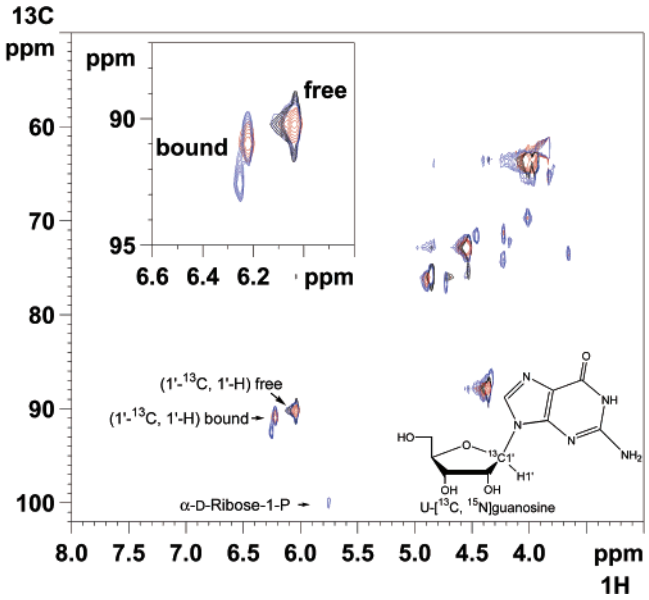

FIGURE 9: ^{1}H, ^{13}C HSQC spectra of U-[^{13}C, ^{15}N]guanosine (black), in the presence of PNP (red), and in the presence of PNP and 2 mM potassium phosphate (blue).

Scheme 3: Binding Equilibria of HGPRTase with Guanosine-5′-phosphate, Pyrophosphate, Guanine, PRPP, and Mg^{2+}

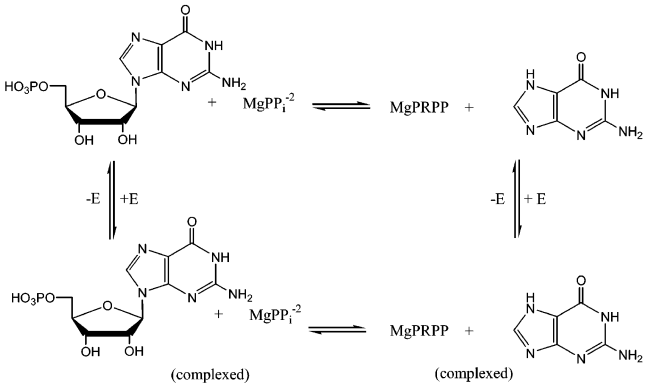

for bound GMP because of Mg^{2+}-pyrophosphate binding despite the formation of the functional Michaelis complexes (Figure 10).

Solid-State NMR Spectra of [1′-^{13}C, 4′-^{15}N]ImmH Free and Bound to Human PNP. Solution NMR did not permit direct observation of the ^{15}N signal from labeled ImmH bound to *M. tuberculosis* PNP. We produced complexes of human PNP•[1′-^{13}C, 4′-^{15}N]ImmH•PO_4 and precipitated them for both ^{13}C- and ^{15}N-solid-state NMR analysis for comparison with precipitates of [1′-^{13}C, 4′-^{15}N]ImmH in neutral and cationic forms. The aliphatic region of the ^{13}C-CP-MAS NMR spectra of labeled ImmH in a neutral (line A) and protonated (line B) state as well as bound to human PNP and phosphate (line C) are shown in Figure 11 (left panel). The frequency of the 1′-^{13}C signal is found to be approximately independent of the protonation state of the neighboring nitrogen atom, as in solution (Figure 3). However, upon binding of the inhibitor to the protein the 1′-^{13}C chemical shift of ImmH increased from 57 to 65 ppm, similar to the solution NMR result with PNP from *M. tuberculosis*. ^{13}C signals resulting from [2-^{13}C, ^{15}N]glycine incorporated into the PNP during expression are found

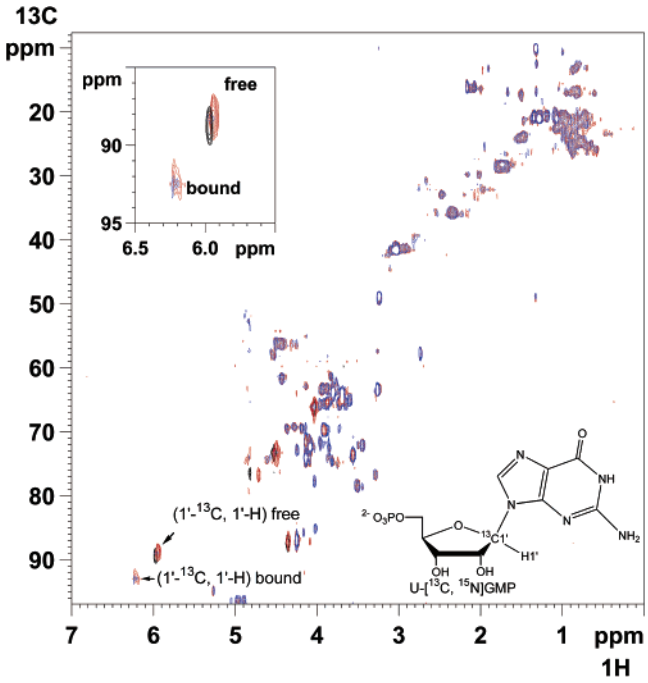

FIGURE 10: ^{1}H, ^{13}C HSQC spectra of U-[^{13}C, ^{15}N]guanosine-5′-monophosphate (black), in the presence of HGPRTase (red), and in the presence of HGPRTase, pyrophosphate, and magnesium chloride (blue).

mainly in the spectral region around 43 ppm and establish formation of the complex.

The ^{15}N-CP-MAS NMR spectra of ImmH in the neutral (spectrum A) and protonated state (spectrum B) and in the complex of human PNP•[1′-^{13}C, 4′-^{15}N]ImmH•PO_4 (spectrum C) are shown in Figure 11 (center panel). In the neutral state, the 4′-^{15}N chemical shift is 51 ppm, and upon protonation the signal is shifted downfield to 57.5 ppm. The line width of the ^{15}N signal is strongly dependent on the crystallization state of the molecule. At pH 8−9 we were able to grow crystals of ImmH that gave a narrower line width than for the cationic inhibitor. The inhibitor bound to the human PNP shows a chemical shift of 61.0 ppm, indicating that the inhibitor is protonated when bound to the protein. The amide backbone signals of isotopically labeled amino acids incorporated into human PNP from [2-^{13}C, ^{15}N]-glycine are found between 100 and 130 ppm. The assignment of the ImmH peak in the protein−inhibitor complex can be confirmed by a DCP experiment that transfers magnetization from the protons to ^{15}N and then to ^{13}C where it is detected. Figure 11 (right panel) shows the DCP spectrum for human PNP•[1′-^{13}C, 4′-^{15}N]ImmH•PO_4 overlayed with the DCP spectra of labeled ImmH in the neutral (green contours) and protonated (blue) state. In concert with the 1-D spectra shown above, the 4′-^{15}N chemical shift of ImmH in the solid state is sensitive to the protonation state, while the 1′-^{13}C shift remains constant upon protonation. In contrast, the 1′-^{13}C signal is shifted downfield upon binding of ImmH to the protein.

DISCUSSION

Transition state structures for *N*-ribosyltransferases have been obtained from kinetic isotope effects (KIEs) and computational chemistry (*9*, *10*, *31*). These enzymes cleave the C−N bond of nucleosides and nucleotides in dissociative

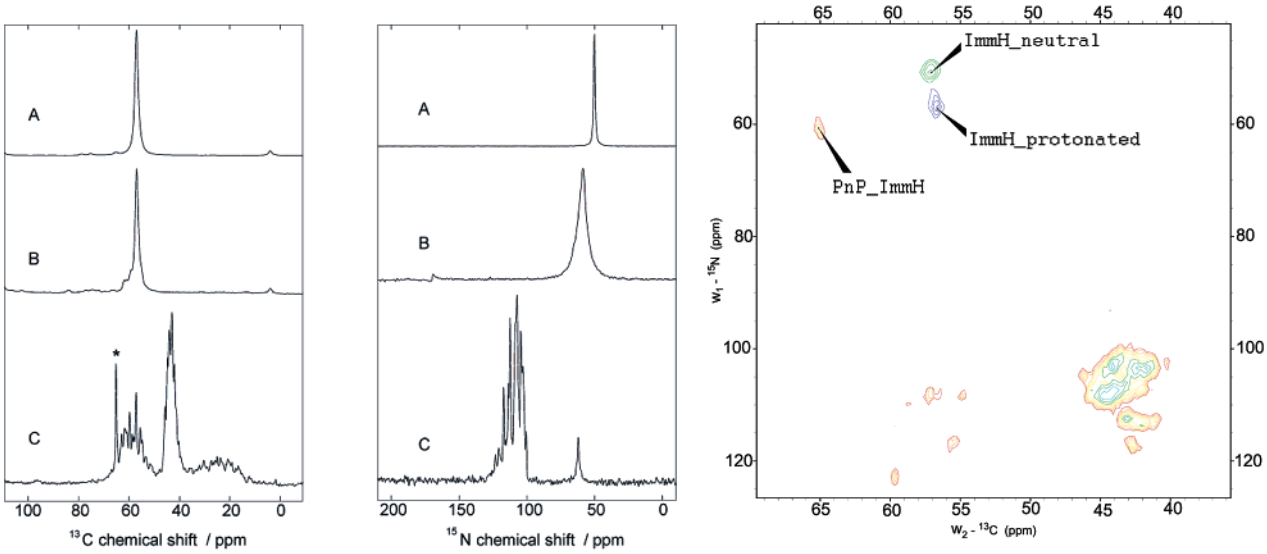

FIGURE 11: (Left panel) Solid state ^{13}C-CP-MAS spectra of [1′-^{13}C, 4′-^{15}N]ImmH in the neutral (A) and protonated (B) state and bound in the complex human PNP•[1′-^{13}C, 4′-^{15}N]ImmH•PO_4 (C). Only the aliphatic regions of the spectra are shown. The ImmH peak in spectrum C is marked by an asterisk. The large change in the chemical shift suggests a conformational strain at C-1′. (middle panel) ^{15}N-CP-MAS spectra of neutral (A) and protonated (A) ImmH and bound to human PNP (C). The chemical shift on the protein suggests a protonated state for the amine. (Right panel) Double CP-MAS spectra of the inhibitor in the neutral (blue) and protonated (green) state overlayed on the DCP spectrum of PNP•ImmH•PO_4.

mechanisms that form transition states with oxacarbenium ion character but only van der Waals interaction with the phosphoryl nucleophiles. Electrostatic stabilization of the oxacarbenium ion by the phosphoryl anion assists transition state formation. The transition state is reached when the *N*-ribosidic bond length has increased by only 0.3−0.4 Å and is followed by a >1.5 Å translocation of the ribosyl C-1′ toward the enzymatically fixed nucleophile (*12*). The purine, the phosphoryl nucleophile, and the 5′-region of nucleosides and nucleotides are fixed during this excursion (*32*). The Immucillins are proposed to mimic the oxacarbenium character of the transition state. It was surprising to find that two *N*-ribosyltransferases bind iminoribitols in their neutral forms and led to the postulate that the cations form in the slow-onset step following binding of the neutral inhibitor (*14*, *23*). This postulate has also been investigated by computational chemistry with the conclusion that protonation of an iminoribitol inhibitor occurs at the catalytic site of nucleoside hydrolase (*36*). Here, we have directly determined the ionization status of Immucillins bound to PNPs and a HGPRTase. Examination of complexes with guanine nucleosides and nucleotides permitted direct comparison of substrate and transition state analogue complexes.

The 4′-imino nitrogen of ImmH and ImmHP can be diprotonated to carry a positive charge as an oxacarbenium ion mimic and the nitrogen at N-7 has an elevated pK_a as a consequence of the 9-deaza modification. These features are also found in the *N*-ribosyltransferase transition states. The affinities of ImmH and ImmHP for PNP and HGPRTase, respectively, exceed those for substrates by factors of 10^4−10^6. Here, we have used solution and solid-state NMR techniques to characterize the ionization of Immucillins in solution and in complexes with two PNPs and a HGPRTase. The chemical shifts of substrate and nucleophilic phosphoryl groups were also measured free and in complex with the enzymes.

pK_a Values for Immucillins. NMR chemical shift analysis of ImmH provided pK_a values for three titratable protons with pK_a values of 1.4, 6.9, and 10 assigned to N-3 of the purine, N-4′ of the iminoribitol and N-7 of the 9-deazapurine. NMR studies of [1′-^{13}C, 4′-^{15}N]ImmH show that the imino nitrogen ^{15}N chemical shift changes from 56.7 to 51.2 ppm upon conversion of the cation to the neutral amine, and the chemical shift behavior was similar for ImmHP. These features were used to probe the nature of enzyme-bound Immucillins.

Ionization State of ImmH Bound to PNP and ImmHP Bound to HGPRTase. Solution NMR spectra of the 1′-H, 1′-^{13}C cross-peaks from PNP•[1′-^{13}C, 4′-^{15}N]ImmH•P_i and HGPRTase•[1′-^{13}C, 4′-^{15}N]ImmHP•$MgPP_i$ gave chemical shifts consistent with the complexed inhibitors existing as the 4′-N cations. In the solid-state, NMR analysis of human PNP directly established that ImmH is present as the cation. Formation of the initial PNP−ImmH complexes mimic the Michaelis complex by binding neutral ImmH with a K_i value in the nM range. Slow-onset inhibition occurs on the enzyme with a rate constant of approximately 0.1 s^{-1} and tightens the binding to the pM range (*13*, *14*). On the basis of the current NMR results, we conclude that the slow-onset step involves protonation at 4′-N for these *N*-ribosyltransferases.

Experimentally unresolved questions for the process of on-enzyme protonation of ImmH include the immediate source of the proton, the reason for preferential binding of the neutral molecule, temporal separation of ImmH protonation relative to the slow-onset conformational change, and the pK_a for ImmH when bound to the enzyme. The ionization state of the unliganded catalytic site is unknown, but for catalytic function with inosine, guanosine, and deoxyguanosine, the enzyme must form Michaelis complexes with neutral molecules. A carboxylate oxygen of E189 in PNP accepts H-bonds from NH-1 and a tightly positioned water and is likely to be ionized in the ImmH complex (Figure 1). If this carboxylate were to be protonated in the unliganded catalytic site, displacement of this proton on substrate binding could provide an immediate proton source. The ionic state of this group has not been spectroscopically analyzed. However, the

slow-onset, tight-binding rate of 0.1 s^{-1} is consistent with a protein conformational change that occurs prior to protonation of ImmH. This slow change could alter the pK_a of bound ImmH and drive protonation from transfer of a water proton. These possibilities provide testable hypotheses for rapid reaction studies while tracking pH changes.

Slow-onset inhibition kinetics of *T. foetus* HGPRTase by ImmHP have not been fully characterized but also involve slow-onset inhibition with a K_i* value of 0.6 nM.[2] Here, both the 1′-H, 1′-^{13}C cross-peak and the direct observation of the ^{15}N chemical shift indicate cationic 4′-N in the tightly bound complex. The HGPRTase•[1′-^{13}C, 4′-^{15}N]ImmHP•$MgPP_i$ complex provided a distinct ^{15}N signal at 58.9 ppm as compared to 51.3 ppm for unprotonated, labeled ImmHP in solution. Bond distortion near nitrogen can also cause chemical shifts. The effects of bond distortion on ^{15}N chemical shifts have been investigated for the tight binding transition state analogues of thermolysin, where changes in ^{15}N chemical shift on/off the enzyme were in the range of 1−4 ppm (*33*). These effects are well below the 7.6 ppm change seen in free/bound ImmHP. These results provide support for the ImmH inhibitors being converted to cationic mimics of the oxacarbenium ion transition states when bound to PNPs and HGPRTase.

Enzymatic Distortion of the Iminoribitol Ring. The chemical shift for 1′-^{1}H of ImmH in solution is 4.30 ppm for the neutral and 4.95 ppm for the cationic state. A further shift downfield to 6.3 ppm occurs in the PNP•[1′-^{13}C, 4′-^{15}N]-ImmH•P_i complex. Additional evidence for distortion at the anomeric carbon is the corresponding 6 ppm downfield chemical shift observed in 1′-^{13}C when bound to the enzyme, despite the lack of a chemical shift change for 1′-^{13}C with 4′-N protonation of Immucillins in solution. This result is almost exactly duplicated in the solid-state NMR spectra of human PNP•[1′-^{13}C, 4′-^{15}N]ImmH•P_i . We propose that this distortion of bound Immucillins toward oxacarbenium geometry is a general feature induced by catalytic site interactions with the PNP enzymes.

Similar results were observed with the complex of HGPRTase•[1′-^{13}C, 4′-^{15}N]ImmHP•$MgPP_i$. Both the 1′-^{1}H and the 1′-^{13}C chemical shifts of ImmHP were highly perturbed on binding and nearly reproduced the results for ImmH binding to PNPs. The 1′-H was located at 6.2 ppm, 1.3 ppm downfield of the extreme of 4′-N protonated ImmHP and 2.2 ppm downfield of the 4′-N neutral species. The 1′-^{13}C chemical shift was downfield of the free solution value by 7 ppm (64.5 vs 57.5 ppm).

As sp^3 carbons are rehybridized toward sp^2, the chemical shift of covalently attached protons moves downfield. The 1′-H and 1′-^{13}C chemical shift changes in going from free to bound cationic Immucillins indicate distortion at 1′-C from sp^3 toward sp^2 hybridization. The transition state for PNP established from kinetic isotope effects is sp^2-like suggesting that the *N*-ribosyltransferases impose sp^2 character on the Immucillins. More perfect transition state analogues might incorporate sp^2 geometry at 1′-C. When presented with a tight-binding transition state analogue with sp^3 geometry at 1′-C, the *N*-ribosyltransferases impose transition state features, an act that requires energy. This distortional binding of the Immucillins prevents them from approaching the theoretical limit of 10^{-18} M dissociation constant for PNPs but emphasizes the ability of enzymes to engage in high-affinity binding when transition state features are present.

Chemical Shift of Bound ^{31}P in Complexes with Immucillins. The ^{31}P NMR spectra of PNP•ImmH•P_i suggests that phosphate is more ionized when bound than free phosphate at the same pH. The change reflects an enzyme-induced shift in the apparent pK_a, altered electron distribution around phosphorus, or both. It is proposed that the altered chemical shift represents increased nucleophilicity of the reacting oxygen. The cationic 4′-N of ImmH is located 3.1 Å from the phosphate anion in PNP and forms an ion pair (Figure 1). A similar ion pair between PO_4 and the ribooxacarbenium ion at the actual transition state is fully consistent with our understanding of the transition state (*12*, *15*).

Bound Mg^{2+}-pyrophosphate ^{31}P signals were well-resolved, establishing that the two phosphoryl groups are in distinct chemical environments at the catalytic site. The most nucleophilic phosphoryl group gives a ^{31}P chemical shift equivalent to free pyrophosphate at a pH >12. The second phosphoryl is in a different environment and is not as deshielded. The NMR experiment does not resolve the assignment of phosphoryl groups, but placement of one oxygen from the −3 ppm phosphoryl near the cationic 4′-N of bound ImmHP provides an ionic pair contributing to binding energy and for transition state stabilization in formation of the ribooxacarbenium ion. Distinct chemical environments for the phosphoryl groups are also evident from crystal structures of HGPRTases where bound PP_i is neutralized by two Mg^{2+} ions (Figure 1).

These chemical shifts can be compared to free PP_i or $MgPP_i$ complexes at equivalent pH values. Free PP_i at pH 7.5 had a chemical shift of −7.3 ppm (Figure 6), while the $MgPP_i$ complex is −4.1 at the same pH. Under these conditions $MgPP_i^{2-}$ is the dominant species, but in the catalytic site two Mg^{2+} ions are in contact with PP_i. Mg^{2+} binding shifts PP_i by 3.1 ppm; therefore, chelation with two Mg^{2+} ions provides sufficient electron withdrawal to account for the observed chemical shift change for bound PP_i but not for the asymmetry. Assignment of the proximal nucleophilic group cannot be made from the present data, but studies with Mg complexes of PRPP may be useful in resolving these assignments.

The bound ImmHP 5′-^{31}P chemical shift was located 1.5 ppm downfield of its solution value of 4.1 ppm reflecting electron withdrawal by the ten H-bonds ≤3.0 Å to bound 5′-phosphate in complexes of HGPRTase•ImmHP•$MgPP_i$ (ref *18;* Figure 1). This interaction immobilizes the 5′-region of substrates through the reaction coordinate and permits 5′-anchoring while 1′-C migrates between base and phosphoryl nucleophiles (*12*, *32*).

Complexes with U-[^{13}C, ^{15}N]Guanosine and GMP. *N*-Ribosyltransferses impose large chemical shift changes when the Immucillins bind. Here, we compare the complexes with Immucillins to those of substrates to establish if ground state (substrate) destabilization is similar to the apparent transition state stabilization seen with the Immucillins. Chemical shifts of U-[^{13}C, ^{15}N]guanosine and U-[^{13}C, ^{15}N]GMP upon binding to PNP and HGPRTase changed less than 0.3 ppm for the 1′-H and less than 3 ppm for 1′-^{13}C. Addition of phosphate

[2] Li, C., Ph.D. Thesis, Albert Einstein College of Medicine, 1999. The K_i* value here is the equilibrium dissociation constant after the slow-onset step has occurred.

or Mg^{2+}-pyrophosphate caused no additional changes, even though chemically equilibrating Michaelis complexes are observed. Large changes for ImmH and ImmHP (1.3−1.4 ppm for 1′-H and 6−7 ppm for 1′-C) at these same positions suggest weak enzyme•ligand interactions with Michaelis complexes and strongly enhanced interactions with the transition state analogues. Both Immucillin complexes feature phosphoryl oxygen anions 3.1 Å from iminoribitol cations to form ion pairs that are also predicted to form in the chemically competent transition state.

Structures of Michaelis and Transition State Analogue Complexes. Crystallographic evidence indicates that PNP and HGPRTase active sites are closed during catalysis by flaps or loops that open to bind substrates (*17*−*19*, *27*). Closing the flap creates new contacts between the Immucillins and the protein (*15*). Comparison of PNP•inosine•SO_4 to PNP•ImmH•PO_4 indicates at least six new H-bonds form with ImmH binding. Similar changes are seen with other *N*-ribosyltransferases (*12*, *15*, *18*, *19*). H/D exchange studies of PNP and HGPRTase with and without Immucillins also establish tighter organization of the protein around the inhibitors (*34*, *35*). Computational dynamics of nucleoside hydrolase with an iminoribitol transition state analogue at the active site also predict protonation of the iminoribitol to the cation as well as decreased active site dynamics (*36*).

CONCLUSIONS

Iminoribitol analogues at the active sites of *N*-ribosyltransferases experience protonation to mimic the transition states and form ion pairs with the incipient nucleophiles. The ionic interaction tightens the catalytic site and associated portions of the protein architecture, but the reaction stalls at this point by virtue of the chemical stability of the Immucillins. Catalytically relevant forces on the bound inhibitor include improved H-bonds to the purine leaving group. The same interactions with the substrate weaken the *N*-ribosidic bond and are responsible for leaving group activation. Downfield 1′-C and 1′-H chemical shift changes indicate that both purine and ribosyl analogues are made electron-deficient by the active site contacts. Ribosyl group activation occurs by the proximity of neighboring group oxygens above and below the ring oxygen. In Immucillins, this environment causes protonation of 4′-N and distortion of 1′-C toward the transition state. Electron expulsion from the ribosyl and withdrawal through the purine facilitates electron flow from the purine ring as it is heterolytically cleaved from the ribosyl group at the transition state.

Transition state analyses of *N*-ribosyltransferases demonstrate that bond order to the nucleophile is minimal. However, our ^{31}P NMR studies indicate that the enzymes activate the phosphoryl nucleophiles. Purine activation, oxacarbenium stabilization, and increased phosphate ionization contribute in concert to catalytic acceleration. A pathway of energetically favored charge migration between purine, oxacarbenium ion, and phosphoryl nucleophile lowers energy along the reaction coordinate, culminating in the migration of the oxacarbenium ion to the nucleophile. This charge migration mechanism explains how charge buildup on the anion assists catalysis while exhibiting minimal bond order at the transition state.

The large chemical shift changes observed for complexes of bound Immucillins, but not substrates, indicate weak interactions in Michaelis complexes but stronger ones with transition state analogues. Strong interactions with transition state analogues do not necessarily establish powerful thermodynamic binding at the actual transition state. Transition state analogues convert a statistically improbable dynamic point on the reaction coordinate near barrier crossing to a static thermodynamic equilibrium where the chemical stability of the analogue traps interactions of the transition state, manifested as tight binding.

REFERENCES

1. Wang, C. C., and Munagala, N. (2002) *Mol. Microbiol. 44*, 1073−1079.
2. Hammond, D. J., and Gutteridge, W. E. (1984) *Mol. Biochem. Parasitol. 13*, 243−261.
3. Sherman, I. W. (1979) *Microbiol. Rev. 43*, 453−495.
4. Kicska, G. A., Tyler, P. C., Evans, G. B., Furneaux, R. H., Kim, K., and Schramm, V. L. (2002) *J. Biol. Chem. 277*, 3219−3225.
5. Kicska, G. A., Tyler, P. C., Evans, G. B., Furneaux, R. H., Schramm, V. L., and Kim, K. (2002) *J. Biol. Chem. 277*, 3226−3231.
6. Schramm, V. L. (2002) *Biochim. Biophys. Acta 1587*, 107−117.
7. Kicska, G. A., Long, L., Horig, H., Fairchild, C., Tyler, P. C., Furneaux, R. H., Schramm, V. L., and Kaufman, H. L. (2001) *Proc. Natl. Acad. Sci. 98*, 4593−4598.
8. Bantia, S., Miller, P. J., Parker, C. D., Ananth, S. L., Horn, L. L., Kilpatrick, J. M., Morris, P. E., Hutchison, T. L., Montgomery, J. A., and Sandhu, J. S. (2001) *Intl. Immunopharm. 1*, 1199−1210.
9. Tao, W., Grubmeyer, C., and Blanchard, J. S. (1996) *Biochemistry 35*, 14−21.
10. Kline, P. C., and Schramm, V. L. (1993) *Biochemistry 32*, 13212−13219.
11. Kline, P. C., and Schramm, V. L. (1995) *Biochemistry 34*, 1153−1162.
12. Federov, A., Shi, W., Kicska, G., Federov, E., Tyler, P. C., Furneaux, R. H., Hanson, J. C., Schramm, V. L., and Almo, S. C. (2001) *Biochemistry 40*, 853−860.
13. Miles, R. W., Tyler, P. C., Furneaux, R. H., Bagdassarian, C. K., and Schramm, V. L. (1998) *Biochemistry 37*, 8615−8621.
14. Basso, L. A., Santos, D. S., Shi, W., Furneaux, R. H., Tyler, P. C., Schramm, V. L., and Blanchard, J. S. (2001) *Biochemistry 40*, 8196−8203.
15. Shi, W., Basso, L. A., Santos, D. S., Tyler, P. C., Furneaux, R. H., Blanchard, J. S., Almo, S. C., and Schramm, V. L. (2001) *Biochemistry 40*, 8204−8215.
16. Miles, R. W., Tyler, P. C., Evans, G. B., Furneaux, R. H., Parkin, D. W., and Schramm, V. L. (1999) *Biochemistry 38*, 13147−13154.
17. Shi, W., Li, C. M., Tyler, P. C., Furneaux, R. H., Grubmeyer, C., Schramm, V. L., and Almo, S. C. (1999) *Nat. Struct. Biol. 6*, 588−593.
18. Shi, W., Li, C. M., Tyler, P. C., Furneaux, R. H., Cahill, S. M., Girvin, M. E., Grubmeyer, C., Schramm, V. L., and Almo, S. C. (1999) *Biochemistry 38*, 9872−9880.
19. Li, C. M., Tyler, P. C., Furneaux, R. H., Kicska, G. A., Xu, Y., Grubmeyer, C., Girvin, M. E., and Schramm, V. L. (1999) *Nat. Struct. Biol. 6*, 582−587.
20. Evans, G. B, Furneaux, R. H., Hutchison, T. L., Kezar, H. S., Morris, P. E., Schramm, V. L., and Tyler, P. C. (2001) *J. Org. Chem. 66*, 5723−5730.
21. Evans, G. B, Furneaux, R. H., Gainsford, G. J., Schramm, V. L., and Tyler, P. C. (2000) *Tetrahedron 56*, 3053−3062.
22. Horenstein, B. A., Zabinski, R. F., and Schramm, V. L. (1993) *Tetrahedron Lett. 34*, 7213−7216.
23. Parkin, D. W., and Schramm, V. L. (1995) *Biochemistry 34*, 13961−13966.
24. Munagala, N. R., and Wang, C. C. (1998) *Biochemistry 37*, 16612−16619.
25. Aronov, A. M., Munagala, N. R., Ortiz de Montellano, P. R., Kuntz, I. D., and Wang, C. C. (2000) *Biochemistry 39*, 4684−4691.
26. Munagala, N. R., Basus, V. J., and Wang, C. C. (2001) *Biochemistry 40*, 4303−4311.

27. Somoza, J. R., Chin, M. S., Foda, P. J., Wang, C. C., and Fletterick, R. J. (1996) *Biochemistry 35*, 7032−7040.
28. Chin, M. S., and Wang, C. C. (1994) *Mol. Biochem. Parasitol. 63*, 221−229.
29. Munagala, N. R., Sarver, A. E., and Wang, C. C. (2000) *J. Biol. Chem. 275*, 37072−37077.
30. Xu, Y., and Grubmeyer, C. (1998) *Biochemistry 37*, 4114−4124.
31. Thomas, A., and Field, M. J. (2002) *J. Am. Chem. Soc. 124*, 12432−12438.
32. Schramm, V. L., and Shi, W. (2001) *Curr. Opin. Struct. Biol. 11*, 657−665.
33. Copie, V., Kolbert, A. C., Drewry, D. H., Bartlett, P. A., Oas, T. G., and Griffin, R. G. (1990) *Biochemistry 29*, 9176−9184.
34. Wang, F., Shi, W., Nieves, E., Angeletti, R. H., Schramm, V. L., and Grubmeyer, C. (2001) *Biochemistry 40*, 8043−8054.
35. Wang, F., Miles, R., Kicska, G., Nieves, E., Schramm, V. L., and Angeletti, R. H. (2000) *Protein Sci. 9*, 1660−1668.
36. Mazumder, D., Kahn, K., and Bruice, T. C. (2002) *J. Am. Chem Soc. 124*, 8825−8833.
37. Fleet, G. J., and Son, J. C. (1988) *Tetrahedron 44*, 2637−2647.
38. Karabinos, J. V. (1963) *Org. Syntheses Coll. 4*, 506−508.
39. Piotto, M., Saudek, V., and Sklenar, V. (1992) *J. Biomol. NMR 2*, 661−665.
40. Wishart, D. S., Bigam, C. G., Yao, J., Abildgaard, F., Dyson, H. J., Oldfield, E., Markey, J., and Sykes, B. D. (1995) *J. Biomol. NMR 6*, 135−140.
41. Bennet, A. E., Rienstra, C. M., Auger, M., Lakshmi, K. V., and Griffin, R. G. (1995) *J. Chem. Phys. 103*, 6951−6958.
42. Schaefer, J., McKay, R. A., and Stejskal, E. O. (1979) *J. Magn. Reson. A 100*, 219−227.
43. Baldus, M., Petkova, A. T., Herzfeld, J., and Griffin, R. G. (1998) *Mol. Phys. 95*, 1197−1207.

BI034003A